Published in IET Microwaves, Antennas & Propagation
Received on 22nd June 2009
Revised on 13th December 2009
doi: 10.1049/iet-map.2009.0365

ISSN 1751-8725

# Accuracy and computational efficiency improvement of ray tracing using line search theory

*V. Mohtashami A.A. Shishegar*

*Department of Electrical Engineering, Sharif University of Technology, Tehran, Iran*
*E-mail: shishegar@sharif.edu*

**Abstract:** This study presents a new ray tracing acceleration technique for site-specific propagation modelling in indoor environments. It overcomes one of the major problems regarding the computational efficiency of shooting-and-bouncing-ray (SBR) method, that is most of the rays emitted from the source do not reach the receiver whereas all of them must be traced. Our proposed method solves this problem in a two-step procedure based on the idea of line search theory. In the first step, called the bracketing phase, the solid angles around the transmitter that transport electromagnetic power to the receiver are determined. In the second step, called the sectioning or zoom phase, the accuracy is improved by iteratively increasing the tessellation frequency of the source in the power-transporting solid angles. No ray will be sent through non-power-transporting solid angles in the sectioning phase. Applying the method to a typical indoor problem is presented and the results are compared with fully 3-D SBR simulation. It is observed that power-transporting solid angles constitute only a small fraction of the total space around the source through which the rays are launched. Therefore a high gain in terms of computational efficiency (about 550–800% saving in the simulation time) is achieved.

## 1 Introduction

Proper design of wireless personal and local area networks requires deep understanding and accurate characterisation of radio wave propagation in indoor environments. Over the past two decades, ray tracing has been widely used for indoor propagation modelling [1–7]. The conventional ray tracing, called the shooting-and-bouncing-ray (SBR) method, uses geometrical optics approximation to model electromagnetic wave propagation in the environment. By using adaptive reception spheres [3], multiple-counting cancellation techniques [8, 9] and ray tube models [4, 7, 10, 11], accurate results can be obtained.

In applications where high accuracy is required, the transmitter must be modelled with a large number of rays. Thus, a heavy computational burden in terms of simulation time is imposed on the SBR algorithm. Reducing the simulation time of the SBR method is still a challenging problem and several acceleration techniques have been proposed in the literature to overcome this drawback. These techniques may be classified into two main categories. The algorithms of the first category focus on reducing the number of intersection tests of the rays with the objects in the environment. This reduction is accomplished by using geometrical algorithms based on the concept of bounding volumes [12, 13]. Bounding volumes are simple geometric objects that are simple to intersect with a ray and surround the objects of the environment in a tree-like manner. Instead of using a brute force method, the algorithm finds the intersected wall through searching in the tree generated by the bounding volumes. This technique significantly reduces the number of intersection tests required. For instance, in [14] the binary space partitioning and in [15] the space volumetric partitioning and angular $Z$-buffer are used whereas in [16, 17] the environment is tessellated using rectangular and triangular meshes, respectively. Since intersection test calculations dominate the run time of the


© The Institution of Engineering and Technology 2010

SBR method, very good speedup can be achieved by applying these techniques.

If the wavefront of a ray hits more than one wall at a single intersection, the computed reflection and transmission coefficients at the intersection point will not accurately describe the electromagnetic interaction of the ray with the intersected wall. This problem is referred to as space sampling error in computer graphics [12] and is depicted for a simple 2-D case in Fig. 1*a*. If a ray intersects a wall at the grazing angle, the probability of space sampling error will increase. The algorithms in the second category of acceleration techniques apply the concept of adaptive super-sampling in computer graphics [12]. They start with a small number of source rays. Whenever the wavefront of a ray hits more than one wall at a single intersection, it is split into smaller wavefronts such that each small wavefront hits only one wall. This situation is depicted in Fig. 1*b* where the wavefront of the parent ray $r_0$ has been split into three child wavefronts corresponding to the rays $r_1$, $r_2$ and $r_3$. The number of child wavefronts generated by the parent wavefront can be determined adaptively as a function of the current sampling rate (current tessellation frequency of the source) and the remaining power in the ray tube. In electromagnetic applications, this method is referred to as ray tube tracing [10] or ray-beam tracing [11]. The sampling of the space (tessellation frequency of the source) is increased only for the rays whose wavefronts hit more than one wall at a single intersection. Thus, run-time saving is achieved.

One of the major drawbacks of the SBR method is that most of the rays emitted from the source do not reach the receiver. Neither of the two categories of acceleration techniques mentioned above is capable of solving this problem. The reason is that the solid angles around the source with contribution to the total electromagnetic field at the receiver remain unknown unless the ray tracing procedure is completed. However, if these solid angles are known a priori, the rays will be launched only through them, resulting in a significant decrease of the computational burden. In this paper, we will present an iterative algorithm to speed up the SBR method based on this idea.

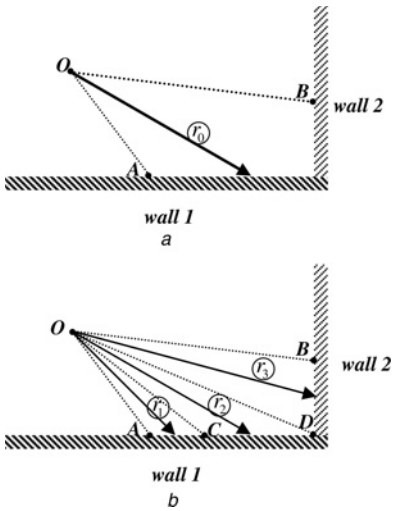


**Figure 1** *Space sampling error and its solution*

*a* Parent ray $r_0$ hits wall 1 whereas its wavefront hits walls 1 and 2
*b* Decomposition of $r_0$ into child rays $r_1$, $r_2$, $r_3$

The original contribution of this paper is the presentation of a novel iterative algorithm for increasing the computational efficiency of the SBR method. This acceleration technique finds the power-transporting solid angles around the source and iteratively increases the tessellation frequency of the source within these solid angles. Note that neither of the two aforementioned categories of acceleration techniques takes the power-transporting solid angles into account. They merely perform specific algorithms on all rays regardless of the contribution at the receiver. In contrast, the acceleration technique of this paper considers the receiver location, and traces the rays only in power-transporting solid angles. Therefore a major portion of unnecessary calculations because of non-power-transporting solid angles is avoided. Moreover, our acceleration technique can be effectively combined with other acceleration techniques that are based on reducing the number of intersection tests. This will further speed up the SBR method. The idea of our acceleration technique is inspired from the line search theory in the area of unconstraint optimisation [18, 19]. This acceleration technique provides significant speedup in typical indoor scenarios.

The paper is organised as follows. Our proposed acceleration technique is presented in Section 2. Numerical results, complexity analysis and processing gain in terms of computational time are reported in Section 3. Finally, conclusions are given in Section 4.

## 2 Acceleration technique

In order to provide a high-resolution ray tracing, we present an iterative algorithm. This algorithm is inspired from the line search theory which is widely used in unconstraint optimisation problems [18, 19]. In the next two subsections, first we will describe the concept of line search. Then, we show how the idea of line search can be applied to improve the computational efficiency and accuracy of the SBR method.

### 2.1 Line search theory

In a typical unconstraint optimisation problem, we wish to minimise a multivariate cost function $f(\boldsymbol{x})$ over the entire $\mathbb{R}^n$ space, where $\boldsymbol{x} \in \mathbb{R}^n$ is the vector of independent variables. The minimisation procedure is usually accomplished in an iterative manner. Suppose $\boldsymbol{x}_k$ is the solution (estimated minimiser) at the start of the $k$th iteration. The updated value of the solution, $\boldsymbol{x}_{k+1}$, may be



© The Institution of Engineering and Technology 2010

computed via the following expression

$$\boldsymbol{x}_{k+1} = \boldsymbol{x}_k + \alpha_k \boldsymbol{p}_k \tag{1}$$

where vector $\boldsymbol{p}_k$ is a descent direction at point $\boldsymbol{x}_k$, which guarantees that $f(\boldsymbol{x})$ can be reduced if we move from $\boldsymbol{x}_k$ along this direction. For instance, $\boldsymbol{p}_k$ can be chosen to be $-\nabla f(\boldsymbol{x}_k)$, where $\nabla f(\boldsymbol{x}_k)$ denotes the gradient of $f(\boldsymbol{x})$ at $\boldsymbol{x}_k$. The scalar $\alpha_k$, which has a positive value, is called the step length. It determines how far to move along $\boldsymbol{p}_k$. There always exists a tradeoff in choosing the step length. We would like to choose $\alpha_k$ to give a substantial reduction of $f$, but at the same time, we wish not to spend so much time on making the choice. The ideal choice would be the global minimiser of the univariate function $\varphi(\alpha)$ defined by

$$\varphi(\alpha) = f(\boldsymbol{x}_k + \alpha \boldsymbol{p}_k), \quad \alpha > 0 \tag{2}$$

This implies that within each step of the main optimisation problem, we are dealing with another optimisation problem that is minimising $\varphi(\alpha)$. In general, however, it is computationally too expensive to minimise $\varphi(\alpha)$ and thus identify the optimal value of the step length. Practical strategies that identify a step length that achieves adequate reduction in $f$ at minimal cost instead of seeking the global minimiser of $\varphi(\alpha)$ are called line search algorithms.

A typical line search algorithm is performed in two stages. In the first stage, called the bracketing phase, an interval $I_0$ containing the exact minimiser of $\varphi(\alpha)$ is found. The second stage, called the sectioning or zoom phase, performs an iterative procedure starting with $I_0$. At each iteration, the initial interval is bisectioned such that only one of the two subsections contains the exact minimiser of $\varphi(\alpha)$. This subsection is passed to the next iteration of the sectioning phase and the procedure is repeated. In other words, we zoom on $I_0$ until we find a small interval containing the exact minimiser of $\varphi(\alpha)$. Any value of $\alpha$ in the final interval can be selected as an estimate of the minimiser of $\varphi(\alpha)$.

## 2.2 Proposed acceleration technique

In the SBR method, it is desirable to model the source with an infinite number of rays. This guarantees accurate reflection and transmission coefficients. Moreover, it ensures that all paths between the transmitter and the receiver are traced and no object in the environment is missed. In practice, however, it is impossible to send out an infinite number of rays. Instead, the source is modelled with a relatively large, but finite number of rays. This implies that there always exists some error in the simulation results. If the number of source rays increases, the error will decrease, but on the other hand, the computational burden in terms of simulation time will also increase. In other words, we are dealing with an optimisation problem in which minimising the cost function (the error in simulation results) is computationally too expensive. In the rest of this subsection, we present an algorithm based on the concept of line search theory to minimise the error at a computationally affordable cost.

In general, the total ray tracing simulation time, denoted by $\Delta t$, can be expressed as

$$\Delta t = n \times \Delta t_n \tag{3}$$

where $n$ is the number of rays emitted from the source (source rays), and $\Delta t_n$ represents the average time required to trace all rays within the binary tree generated by a single source ray. The term 'binary tree' refers to the tree-like sequence of rays generated by a source ray at the consecutive intersections with the walls of the environment. Each source ray represents a small solid angle around the source and transports some part of its radiated power. The conventional SBR algorithm traces the rays within the binary trees generated by all source rays. However, only a few numbers of binary trees usually contribute to the total electromagnetic field at the receiver. Therefore the field at the receiver can be computed by tracing only the binary trees of the power-transporting solid angles. Consequently, a significant decrease in the simulation time can be obtained. Equivalently, the source can be modelled with a very large number of source rays, but the SBR algorithm traces only the binary trees of the source rays within power-transporting solid angles. Thus, the error in the simulation results (caused by modelling the source with finite number of rays) can be minimised within an acceptable simulation time.

*2.2.1 Source model:* The source model used in our acceleration technique is taken from [3]. This method uses an icosahedron inscribed in a sphere around the source. The radius of this sphere is determined by the far-field region of the transmitting antenna. A typical icosahedron with 20 identical equilateral triangular faces is depicted in Fig. 2*a*. To achieve a higher resolution in terms of angular separation between the adjacent rays, each edge of the icosahedron is divided into $N$ equal segments. Afterwards,

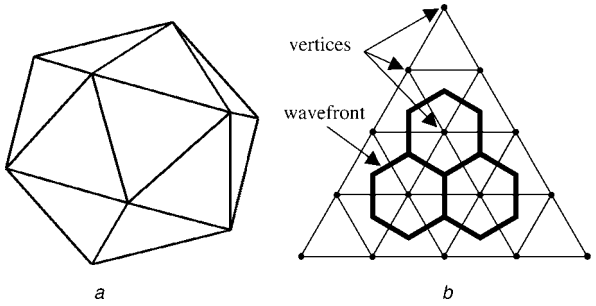


**Figure 2** *Source model*

*a* A typical icosahedron with 20 identical equilateral triangular faces

*b* Tessellation of one face with the tessellation frequency of $N = 4$


*IET Microw. Antennas Propag.*, 2010, Vol. 4, Iss. 9, pp. 1290–1299
© The Institution of Engineering and Technology 2010
doi: 10.1049/iet-map.2009.0365

lines parallel to the edges are drawn and form a tessellated face as shown in Fig. 2*b* for $N = 4$. The rays with hexagonal wavefronts are launched in the direction from the source to the vertices that are generated on the icosahedron faces. Since the icosahedron is geometrically symmetrical around its centre, in which the phase centre of the transmitting antenna is located, the source rays are uniformly generated with similar wavefronts and nearly identical angular separation. The parameter $N$ is called the tessellation frequency. The total number of generated source rays is $10N^2 + 2$. Thus, the tessellation frequency controls the resolution of the source model.

*2.2.2 Bracketing phase:* We now use the idea of line search to improve the computational efficiency of the SBR method. The flowchart of our acceleration technique is depicted in Fig. 3. It is composed of bracketing and sectioning stages similar to the traditional line search. In the bracketing phase, the power-transporting solid angles around the source are determined. Then, the sectioning

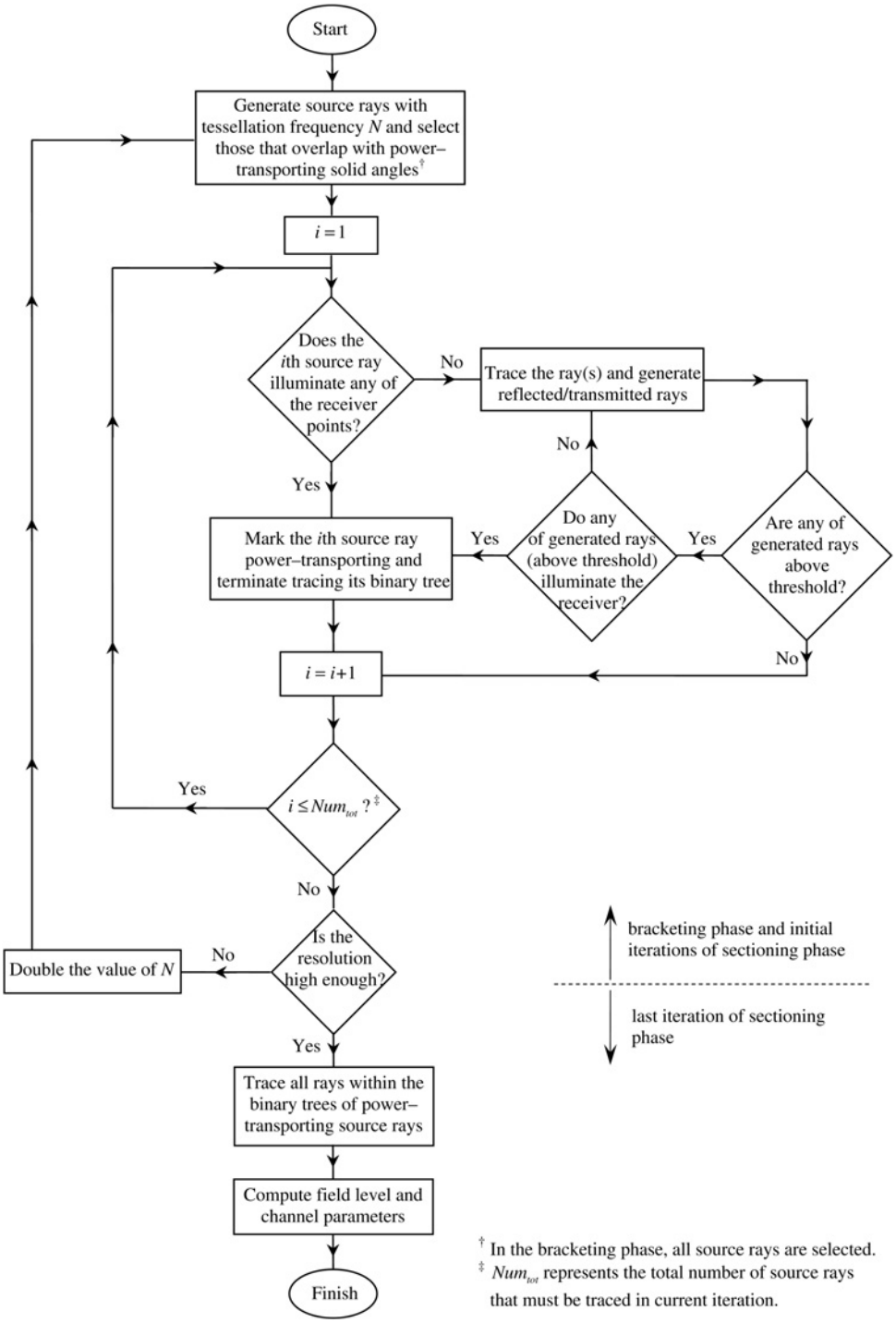


**Figure 3** *Flowchart of proposed acceleration technique*



© The Institution of Engineering and Technology 2010

phase improves the accuracy by iteratively increasing the tessellation frequency of the source in power-transporting solid angles. No rays are sent out in non-power-transporting solid angles in the sectioning phase.

The bracketing phase starts by modelling the source with a relatively low tessellation frequency. Therefore a few source rays are generated each of which representing a nearly large solid angle. Then, the SBR method is used to trace the source rays. Consider the first source ray. If the wavefront of this ray illuminates the location of the receiver, it is marked as a power-transporting source ray and is passed to the sectioning phase. Otherwise, it is traced and the corresponding reflected and transmitted rays are calculated. Now, we check whether the wavefronts of the reflected and transmitted rays illuminate the receiver location. If the receiver falls within at least one of the wavefronts, the first source ray is marked as power-transporting and passed to the sectioning phase. Otherwise, the reflected and transmitted rays are traced. Each of these two rays generates a reflected ray and a transmitted ray. Thus, we now have four rays to deal with. We check these rays for probable illumination of the receiver. If at least one of them illuminates the receiver, the first source ray is marked as power-transporting and is passed to the sectioning phase. Otherwise, these rays are traced. This procedure is repeated until either the first source ray is found to be power-transporting or the magnitude of all generated rays in the binary tree falls below a predefined threshold without illuminating the receiver.

The rest of the source rays are treated in the same manner as discussed above. We emphasise that the goal of the bracketing phase is to determine the power-transporting solid angles. Utilising the above procedure, the rays within the binary tree of a source ray are traced only if the source ray has not been marked as power-transporting till that specific time. Therefore the ray tracing procedure in the bracketing phase is computationally very efficient. It can be observed in Fig. 3 that during the bracketing phase and the initial iterations of the sectioning phase, the amplitude of the electric field of each ray must be checked to be above the predefined threshold prior to illumination test at the receiver.

*2.2.3 Sectioning phase:* The goal of the sectioning phase is to improve the accuracy. We note that power-transporting solid angles are determined in the bracketing phase. The rest of solid angles (non-power-transporting solid angles) do not contribute to the electromagnetic field at the receiver. To increase the accuracy, the wavefronts of power-transporting source rays must be decomposed into smaller wavefronts. This will guarantee more accurate reflection and transmission coefficients at each intersection of the rays with the objects in the environment as well as more accurate paths towards the receiver. The choice of the decomposition scheme determines the computational burden of the sectioning phase. One efficient way of wavefront decomposition is to generate the source rays with higher tessellation frequency, but tracing only those rays whose wavefronts overlap, even partly, with power-transporting wavefronts. A deeper insight can be obtained by referring to Fig. 4. Suppose that we have modelled the source with $N = 4$ in the bracketing phase and the dark solid angle in Fig. 4*a* has been found to be power-transporting. At the start of the sectioning phase, the icosahedron faces are tessellated with $N = 8$ to achieve higher resolution as shown in Fig. 4*b*. The wavefronts of the newly generated source rays are the small hexagons. The dark power-transporting wavefront is also shown in this figure. As observed, seven small hexagons overlap with the dark power-transporting wavefront. Therefore the rays corresponding to these seven hexagonal wavefronts must be traced.

The newly generated source rays whose wavefronts overlap with power-transporting wavefronts are traced using the procedure described in the bracketing phase. At the end of the tracing procedure, the power-transporting solid angles

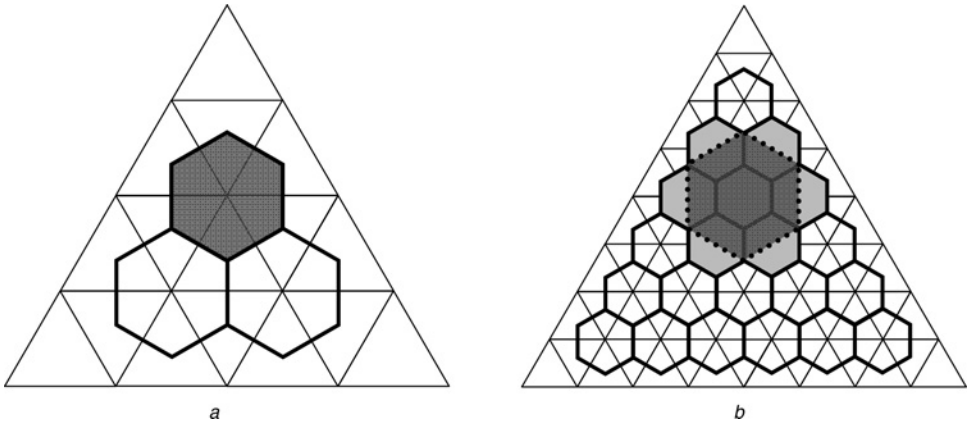


**Figure 4** *Wavefront decomposition by doubling the tessellation frequency*

*a* Source is modelled with the tessellation frequency of $N = 4$. The dark wavefront is marked power-transporting
*b* Source is modelled with the tessellation frequency of $N = 8$. The dark wavefront overlaps with seven lightly shaded small wavefronts


© The Institution of Engineering and Technology 2010
doi: 10.1049/iet-map.2009.0365

with $N = 8$ are determined. Now, we repeat the above procedure to achieve even better resolution. The wavefronts of power-transporting solid angles (with $N = 8$) are determined on the icosahedron faces. Then, the source rays are generated with a higher tessellation frequency, for example, with $N = 16$. The source rays whose wavefronts overlap with power-transporting wavefronts are traced using the procedure described in the bracketing phase. In other words, the sectioning phase improves the accuracy by iteratively increasing the tessellation frequency of the source in power-transporting solid angles.

The sectioning phase continues until the source is modelled with a high enough tessellation frequency. However, as can be observed in Fig. 3, in the last iteration of the sectioning phase we perform a complete ray tracing of the source rays that must be traced, that is all rays within the binary trees of these source rays are traced regardless of their contribution at the receiver. The reason is that the electric field level and other wireless channel parameters are supposed to be computed at the end of the last iteration of the sectioning phase. Hence, the complete information of all rays within the binary trees of power-transporting source rays is required. In other words, the goal of the last iteration of the sectioning phase is different from that of the bracketing phase and the previous iterations of the sectioning phase (for which the only goal was to determine power-transporting solid angles). When the magnitude of all rays falls below the threshold, the ray detection test and multiple-counting cancellation are fulfilled. Now, the field level and wireless channel parameters can readily be obtained in the post-processing stage. We emphasise that power-transporting solid angles constitute only a very small fraction of the total space around the transmitter. Therefore our proposed acceleration technique improves the accuracy at an affordable cost.

*2.2.4 Computational complexity:* The increment coefficient is an important measure of the computational burden of our proposed method. It is defined as the ratio of the total number of small wavefronts (in a new iteration of the sectioning phase) that overlap with the large power-transporting wavefronts (already detected in the bracketing phase or the previous iteration of the sectioning phase). For instance, if the dark wavefront of Fig. 4*b* is the only power-transporting wavefront in the bracketing phase or the previous iteration of the sectioning phase, the increment coefficient is seven. This means that seven rays corresponding to the lightly shaded small wavefronts must be traced in the next iteration of the sectioning phase. The lesser the increment coefficient is, the smaller the number of rays that must be traced in the next iteration of the sectioning phase. The value of increment coefficient depends on the amount of increase in the tessellation frequency. The total number of generated source rays equals $10N^2 + 2$, which is almost proportional to the square of the tessellation frequency for typical values of $N$. Thus, the area of hexagonal wavefronts has a $1/N^2$ dependence which means that the optimal value of the increment coefficient is the square of the ratio of the new tessellation frequency to the old one. For instance, the optimal value of the increment coefficient of the case shown in Fig. 4 is $(8/4)^2 = 4$ whereas its actual value is 7. The partial overlapping of the dark wavefront with the small wavefronts accounts for the deviation of the increment coefficient from its optimal value.

The value of the increment coefficient can be reduced by one unit if we double the tessellation frequency from one iteration to the next. As we can see in Fig. 4*b*, the centre of the power-transporting wavefront lies exactly on the centre of the totally overlapped small wavefront behind it. This implies that the ray corresponding to this small wavefront is exactly the same as that of the dark wavefront. Since the ray of the dark wavefront was traced in the last iteration, it is not necessary to trace the small wavefront. Thus, the increment coefficient reduces to 6.

The increment coefficient is a function of the number of adjacent power-transporting solid angles as well. Suppose that all three wavefronts of the interior vertices of Fig. 4*a* have been marked as power-transporting. If the tessellation frequency is doubled as shown in Fig. 5, only 15 rays must be traced in the next iteration. This implies an increment coefficient of five. The increment coefficient is a descending function of the number of adjacent power-transporting solid angles. We will see in the next section that for typical indoor environments, doubling the tessellation frequency results in an increment coefficient between four and five. This value is a little more than the optimal value resulting in an acceptable computational burden.

## 3 Numerical results

To validate our proposed method, a fully 3-D ray tracing code is prepared first. It is important to validate our code prior to presenting numerical results regarding our proposed acceleration technique. To achieve this goal, an electromagnetic problem with an available analytical solution is taken into account and the ray tracing results are compared to this solution. Fig. 6*a* depicts a 5-GHz vertically polarised half-wavelength dipole antenna that

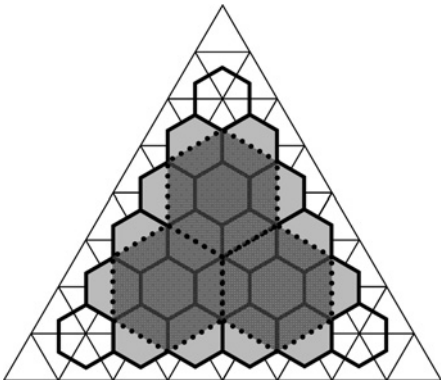

**Figure 5** *Increment coefficient decreases when adjacent solid angles are detected at the receiver*



© The Institution of Engineering and Technology 2010

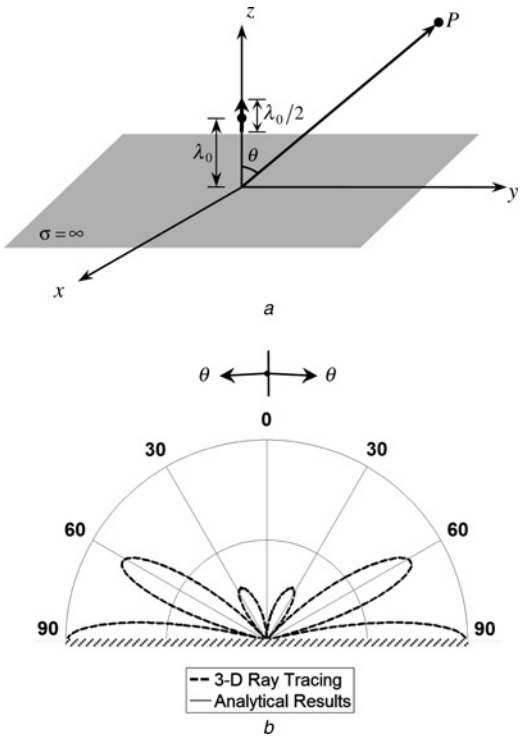


**Figure 6** *Validation of the SBR method*

*a* A 5-GHz half-wavelength dipole antenna located above a PEC
*b* Magnitude of normalised far-field radiation pattern of the antenna

radiates in free space. It is located one wavelength above an infinite perfect electric conductor (PEC). The far-field electric field of the antenna is calculated by applying the image theory [20]

$$\boldsymbol{E}(r,\theta,\phi) = 2\sqrt{\frac{\eta_0 P_{\text{rad}} G}{2\pi}}\frac{\cos((\pi/2)\cos\theta)\cos(2\pi\cos\theta)}{\sin\theta} \times \frac{\mathrm{e}^{-\mathrm{j}k_0 r}}{r}\hat{\theta} \quad (4)$$

where $P_{\text{rad}}$ is the radiated power and $G$ is the gain of the transmitting antenna. Moreover, $\eta_0$ and $k_0$ are the intrinsic impedance and the propagation constant of the free space, respectively. Clearly, the electric field described by (4) is valid only for $0 \leq \theta < \pi/2$.

Fig. 6*b* shows the magnitude of the normalised far-field radiation pattern calculated by the analytical solution presented in (4) as well as the result of high-resolution ray tracing simulation. A good agreement between the two curves is observed. The mean of the relative difference between the two curves is computed to be less than 1%. Therefore our ray tracing code is working properly.

After code validation, our proposed acceleration technique is applied to the indoor propagation in the building shown in Fig. 7. This figure shows the first floor of a building formed by two identical storeys [21]. A vertically polarised

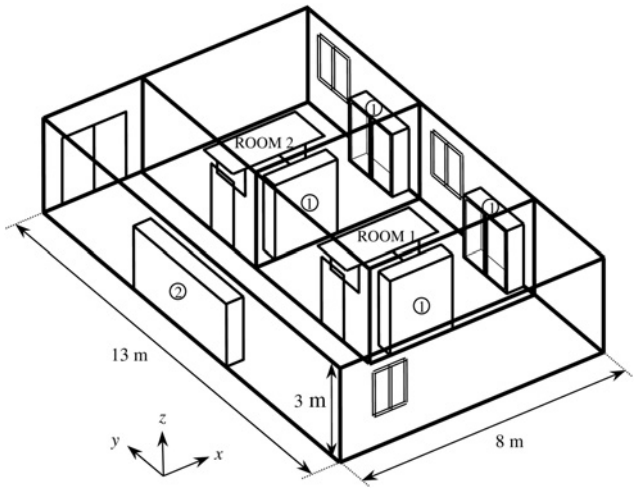


**Figure 7** *Plan of the first floor of a building formed by two identical storeys [21]*

Transmitter is located at Room 1 just above the door

half-wavelength dipole antenna operating at 2.44 GHz and radiating 10 mW is used as the transmitter. It is located at Room 1 just above the door at point ($x = 3.08$ m, $y = 4.52$ m and $z = 2.6$ m). There are wooden doors and tables, wooden and metallic cabinets and glass windows in the building. The wooden cabinets are labelled 1 and the metallic cabinet is labelled 2. The electrical properties of the materials and thicknesses of the slabs used in the simulation are listed in Table 1 according to [21]. The electric field magnitude and the rms delay spread of the power delay profile of the radio channel are calculated by using our proposed acceleration technique. The results are then compared to those of the fully 3-D ray tracing. Both line-of-sight (LOS) and non-line-of-sight (NLOS) cases are considered. For the LOS case, the channel parameters are calculated in Room 1 for 50 equidistant points along a line at ($x = 4$ m, 3.8 m $< y <$ 7.8 m and $z = 1.05$ m). The NLOS case is considered for 50 equidistant points along the line at ($x = 1$ m, 5 m $< y <$ 12 m and $z = 1.2$ m) in the corridor. In our acceleration technique, the tessellation frequency of the source in the bracketing phase is selected as $N = 15$, which is doubled at each iteration of the sectioning phase. The sectioning phase is repeated three times resulting a final tessellation frequency of $N = 120$. The Turin's model based

**Table 1** Material properties and slab thicknesses [21]

| | $\varepsilon_r$ | $\sigma$ (mS/m) | Thickness (cm) |
|---|---|---|---|
| ceiling/floor | 7.9 | 89 | 25.0 |
| external brick wall | 5.2 | 28 | 22.0 |
| internal brick wall | 5.2 | 28 | 12.0 |
| wooden door/ cabinet/table | 3.0 | 0 | 4.0 |
| glass window | 3.0 | 0 | 0.5 |


© The Institution of Engineering and Technology 2010
*IET Microw. Antennas Propag.*, 2010, Vol. 4, Iss. 9, pp. 1290–1299
doi: 10.1049/iet-map.2009.0365

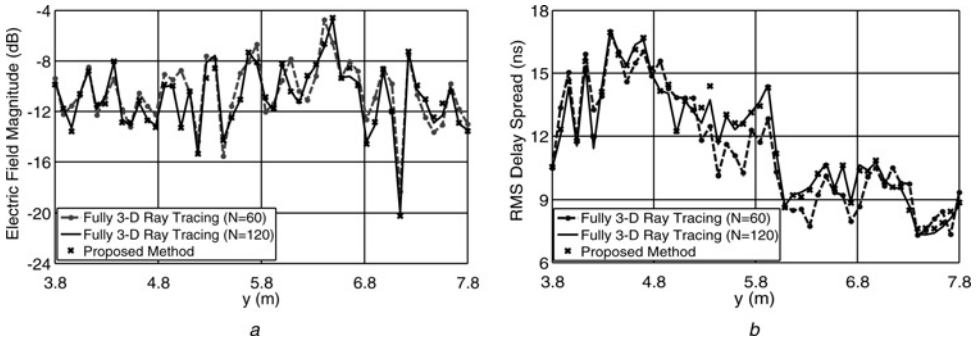


**Figure 8** *Radio channel parameters computed by our proposed method and fully 3-D ray tracing with N = 60 compared to the reference solution (fully 3-D ray tracing with N = 120) for LOS case*

*a* Electric field magnitude
*b* rms delay spread

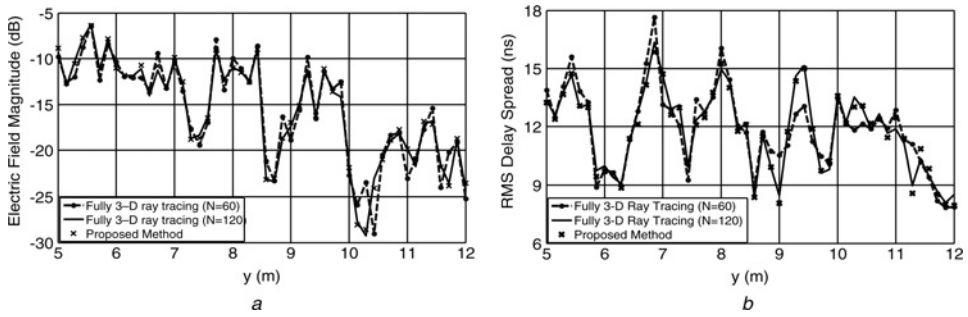


**Figure 9** *Radio channel parameters computed by our proposed method and fully 3-D ray tracing with N = 60 compared to the reference solution (fully 3-D ray tracing with N = 120) for NLOS case*

*a* Electric field magnitude
*b* rms delay spread

on finite duration Gaussian pulses is used to calculate the rms delay spread of the power delay profile of the radio channel [22]. A fully 3-D ray tracing with tessellation frequency of $N = 120$ is considered as the reference solution. In each tracing procedure, the rays are traced until their magnitude falls below the predefined threshold. This threshold is chosen to be 50 dB below the magnitude of the strongest source ray at the reference distance of 1 m away from the transmitting antenna. The results are depicted in Figs. 8 and 9 for LOS and NLOS cases, respectively. Excellent agreement between the results is observed. There is, however, a little difference between the results. The source of the difference will be discussed later in this section.

All of the cases previously discussed were simulated by using a MATLAB code on a PC with Intel core 2 Duo, 3 GHz CPU and 4 GB of RAM. The processing gain and difference characteristics for both LOS and NLOS cases are summarised in Table 2. Processing gain is defined as the ratio of the simulation time of the reference solution to the simulation time of our proposed acceleration technique. It shows the amount of speedup obtained by applying our acceleration technique. The difference between the electric field magnitude (in dB) resulting from our proposed method and that of the reference solution is computed at each receiving point. These values are then used to obtain the mean ($M$) and standard deviation (SD) of the difference using the following equations

$$M = \frac{1}{n}\sum_{i=1}^{n} \left| |\boldsymbol{E}_{\mathrm{R}}^{i}| - |\boldsymbol{E}_{\mathrm{P}}^{i}| \right| \tag{5}$$

$$\mathrm{SD} = \left[ \frac{1}{n}\sum_{i=1}^{n} \left( |\boldsymbol{E}_{\mathrm{R}}^{i}| - |\boldsymbol{E}_{\mathrm{P}}^{i}| \right)^2 \right]^{1/2} \tag{6}$$

where $n$ is the number of receiving locations, and $\boldsymbol{E}_{\mathrm{R}}^{i}$ and $\boldsymbol{E}_{\mathrm{P}}^{i}$ denote the total electric field vector at the $i$th receiving location computed by the reference solution and by our proposed acceleration technique, respectively. A high processing gain and acceptable difference characteristics are achieved. The processing gain depends on various parameters such as the termination threshold for the rays, losses of the walls and the number of receiving locations. In both LOS and NLOS cases simulated above, 50 points are considered as receiver locations. If results are to be computed for a smaller number of locations, the processing gain increases even more. This is because a smaller number of source rays will be detected at the receiver locations in each iteration of the algorithm. On the other hand, if the number of receiving locations increases, as is the case in radio planning, the simulation speedup is reduced. For a typical spatial resolution of 1 m × 1 m, the simulation



© The Institution of Engineering and Technology 2010

**Table 2** Processing gain and difference characteristics of our proposed method compared to the reference solution

| | LOS path | NLOS path |
|---|---|---|
| number of receiving locations | 50 | 50 |
| total number of traced source rays in reference solution | 144 002 | 144 002 |
| total number of traced source rays in proposed method | 22 872 | 13 274 |
| processing gain, % | 545 | 794 |
| average increment coefficient | 4.45 | 4.51 |
| electric field mean difference (dB) | 0.22 | 0.28 |
| electric field difference standard deviation (dB) | 0.26 | 0.29 |

speedup of the environment of Fig. 7 with the same input data as described above is reduced to 240%. However, the speedup is still noticeable. Furthermore, the proposed acceleration technique works well in situations where there are 'blind zones' (locations with very weak signal power) in the environment. In those cases, some compensation techniques such as minor changes in the location of the access point are performed by the system designer to improve the signal level in the blind zones. Therefore a limited number of points located in the blind zones needs to be checked after the compensation is done. A fast ray tracing simulation based on the proposed acceleration technique will be a very good choice for this purpose.

According to Table 2, the average value of the increment coefficient in the three iterations of the algorithm is almost 4.5. This is just a little above the optimal value of 4 that results in an acceptable computational burden.

In Figs. 8 and 9, two other graphs are depicted which show the results of a fully 3-D ray tracing simulation with a lower tessellation frequency, that is, with $N = 60$. This tessellation frequency is selected because its simulation time almost equals the simulation time of our proposed method. Table 3 compares the difference characteristics of these two results with respect to the reference solution. It is evident from Figs. 8, 9 and Table 3 that the result of our proposed method follows the reference solution much better than that of fully 3-D ray tracing simulation with $N = 60$. Therefore for the same simulation time, our proposed method performance is much better than a fully 3-D ray tracing simulation with a lower tessellation frequency.

**Table 3** Results of our proposed method and fully 3-D ray tracing with $N = 60$ compared to the reference solution

| | LOS path | NLOS path |
|---|---|---|
| electric field mean difference of fully 3-D ray tracing with $N = 60$ (dB) | 1.04 | 1.14 |
| electric field mean difference of proposed method (dB) | 0.22 | 0.28 |
| electric field difference standard deviation of fully 3-D ray tracing with $N = 60$ (dB) | 0.81 | 1.24 |
| electric field difference standard deviation of proposed method (dB) | 0.26 | 0.29 |

The source of the difference between the results of our proposed method and the reference solution is the well-known problem of large wavefronts. Since the bracketing phase starts with rather a low tessellation frequency, the wavefronts of the rays are relatively large. Hence, it is probable that the wavefronts of some rays hit more than one wall at some intersections. This problem can be fully solved by using the adaptive ray tube tracing (ADRTT) method [10] or ray-beam tracing [11]. In these methods, a ray tube that hits more than one wall is split into several ray tubes such that each newly generated ray tube hits only one wall. This situation was depicted in Fig. 1 earlier in this paper. We applied these methods to our proposed algorithm and eliminated the difference, but it reduced the processing gain significantly. For the LOS and NLOS cases described above, the speedup decreased from 545% and 794% to 103% and 105%, respectively, although complete cancellation of the difference with respect to the results of the reference solution was observed. However, the difference between our results and the reference solution is very small and can be absolutely neglected for engineering purposes. Therefore it is suggested that our proposed method be performed without ADRTT or ray-beam tracing techniques. Instead, the tessellation frequency in the bracketing phase should be selected properly (neither very low nor very high). The proper choice of tessellation frequency in the bracketing phase depends on the complexity of the indoor environment. A more complex case requires a higher tessellation frequency. However, a number between 10 and 20 seems to be a proper choice according to the authors' experiences.

## 4 Conclusions

A new acceleration technique for the ray tracing algorithm based on the idea of line search theory is presented in this paper. Instead of reducing the number of intersection tests, our proposed method reduces the number of traced source rays by finding the solid angles around the transmitter that transport electromagnetic power to the receiver. Then, high-resolution rays are sent out only in these solid angles and the procedure continues iteratively until a high enough resolution is achieved. Since a few rays are traced in each iteration, high resolution can be achieved within an acceptable simulation time. A small difference between the results of our proposed method and the fully 3-D


© The Institution of Engineering and Technology 2010
*IET Microw. Antennas Propag.*, 2010, Vol. 4, Iss. 9, pp. 1290–1299
doi: 10.1049/iet-map.2009.0365

simulation is observed. However, with the proper choice of initial tessellation frequency, the difference is absolutely negligible and the results are reliable for engineering purposes. A high processing gain in terms of simulation time is achieved. Our proposed method is different in its foundations from other acceleration techniques that have been previously presented in the literature. There will be no conflict if it is used simultaneously with other acceleration techniques which are based on reducing the number of intersection tests. Preparing such a super-efficient and accurate ray tracing code will be the next step in this research.

## 5 Acknowledgment

The authors wish to thank Iran Telecommunication Research Center (ITRC) for supporting this research under the contract T/500/8524.

## 6 References

[1] MCKOWN J.W., HAMILTON R.L. JR.: 'Ray tracing as a design tool for radio networks', *IEEE Netw. Mag.*, 1991, **5**, pp. 27–30

[2] HO C.M.P., RAPPAPORT T.S.: 'Wireless channel prediction in a modern office building using an image-based ray tracing method'. IEEE GLOBECOM '93, Houston, TX, November 1993, pp. 1247–1251

[3] SEIDEL S.Y., RAPPAPORT T.S.: 'Site-specific propagation prediction for wireless in-building personal communication system design', *IEEE Trans. Veh. Technol.*, 1994, **43**, pp. 879–891

[4] YANG C.F., WU B.C., KO C.J.: 'A ray-tracing method for modeling indoor wave propagation and penetration', *IEEE Trans. Antennas Propagat.*, 1998, **46**, pp. 907–919

[5] ADANA F.S., BLANCO O.G., DIEGO I.G., ARRIAGA J.P., CÁTEDRA M.F.: 'Propagation model based on ray tracing for the design of personal communication systems in indoor environments', *IEEE Trans. Veh. Technol.*, 2000, **49**, pp. 2105–2112

[6] TARNG J.H., CHANG W.R., HSU B.J.: 'Three-dimensional modeling of 900 MHz and 2.44 GHz radio propagation in corridors', *IEEE Trans. Veh. Technol.*, 1997, **46**, pp. 519–527

[7] CHEN S.-H., JENG S.-K.: 'An SBR/Image approach for radio wave propagation in indoor environments with metallic furniture', *IEEE Trans. Antennas Propagat.*, 1997, **45**, pp. 98–106

[8] NOORI N., SHISHEGAR A.A., JEDARI E.: 'A new double counting cancellation technique for three-dimensional ray launching method'. IEEE Antennas Propagat. Soc. Int. Symp., Albuquerque, NM, July 2006, pp. 2185–2188

[9] MOHTASHAMI V., SHISHEGAR A.A.: 'A new double-counting cancellation technique for ray tracing using separation angle distribution'. IEEE Radio Frequency and Microwave (RFM) Conf., Kuala Lumpur, Malaysia, December 2008, pp. 437–441

[10] SUZUKI H., MOHAN A.S.: 'Ray tube tracing method for predicting indoor channel characteristics map', *Electron. Lett.*, 1997, **33**, pp. 1495–1496

[11] RAJKUMAR A., NAYLOR B.F., FEISULLIN F., ROGERS L.: 'Predicting RF coverage in large environments using ray-beam tracing and a partitioning tree represented geometry', *Wirel. Netw.*, 1996, **2**, (2), pp. 143–154

[12] GLASSNER S.: 'An introduction to ray tracing' (Academic Press, 1989)

[13] GOLDSMITH J., SALMON J.: 'Automatic creation of object hierarchies for ray tracing', *IEEE Comput. Graph. Appl.*, 1987, **7**, (5), pp. 14–20

[14] TORRES R.P., VALLE L., DOMINGO M., LOREDO S.: 'An efficient ray-tracing method for radiopropagation based on the modified BSP algorithm'. IEEE Vehicular Technology Conf. (VTS 50th), Amsterdam, Netherlands, September 1999, vol. 4, pp. 1967–1971

[15] CÁTEDRA M.F., PÉREZ J., ADANA F.S., GUTIÉRREZ O.: 'Efficient ray-tracing technique for three-dimensional analyses of propagation in mobile communications: application to picocell and microcell scenarios', *IEEE Antennas Propagat. Mag.*, 1998, **40**, (2), pp. 15–28

[16] ZHENGQING Y., ISKANDER M.F., ZHIJUN Z.: 'Fast ray tracing procedure using space division with uniform rectangular grid', *Electron. Lett.*, 2000, **36**, (10), pp. 895–897

[17] ZHENGQING Y., ISKANDER M.F., ZHIJUN Z.: 'A fast indoor/outdoor ray tracing procedure using combined uniform rectangular and unstructured triangular grids'. IEEE Antennas Propagat. Soc. Int. Symp., Salt Lake City, UT, July 2000, vol. 2, pp. 1134–1137

[18] NOCEDAL J., WRIGHT S.J.: 'Numerical optimization' (Springer–Verlag, 1999)

[19] FLETCHER R.: 'Practical methods of optimization' (Wiley, 1980)

[20] BALANIS C.A.: 'Antenna theory, analysis and design' (Wiley, 2005)

[21] BERNARDI P., CICCHETTI R., TESTA O.: 'An accurate UTD model for the analysis of complex indoor radio environments in microwave WLAN systems', *IEEE Trans. Antennas Propagat.*, 2004, **52**, (6), pp. 1509–1520

[22] HASHEMI H.: 'The indoor radio propagation channel', *Proc. IEEE*, 1993, **81**, pp. 943–968



© The Institution of Engineering and Technology 2010